 doi:10.20944/preprints202101.0564.v1

Article

Fischer-Tropsch Synthesis as Key for a Decentralized Sustainable Kerosene Production

Andreas Meurer [1,*] and Jürgen Kern [1]

[1] Department of Energy Systems Analysis, Institute of Engineering Thermodynamics, German Aerospace Center (DLR), Curiestraße 4, 70563 Stuttgart, Germany; juergen.kern@dlr.de
* Correspondence: andreas.meurer@dlr.de; Tel.: +49-711-6862-8100

Abstract: Synthetic fuels play an important role in the defossilization of future aviation transport. To reduce the ecological impact of remote airports due to long range transportation of kerosene, a decentralized on-site-production of synthetic paraffinic kerosene is applicable, preferably as near-drop-in fuel or alternatively as blend. One possible solution for such a production of synthetic kerosene is the Power-to-Liquid process. The basic development of a simplified plant layout addressing the specific challenges of a decentralized kerosene production which differ from most current approaches for infrastructural well-connected regions is described. The decisive influence of the Fischer-Tropsch synthesis on the PtL process is shown by means of a steady-state reactor model which was developed in Python and serves as basis for further development of a modular environment able to represent entire process chains. The reactor model is based on reaction kinetics according current literature. The effects of adjustments of the main operation parameters on the reactor behavior are evaluated and the impacts on up- and downstream processes are described. The results prove the governing influence of the Fischer-Tropsch reactor on the PtL process and show its flexibility regarding the desired product fraction output, which makes it an appropriate solution for a decentralized kerosene production.

Keywords: alternative fuels; power-to-liquid; synthetic fuel; synthetic kerosene; aviation fuel; sustainable fuel; power-to-x; e-fuel; fischer-tropsch; renewable fuel

1. Introduction

1.1. Motivation

An annual increase of over 4% on average is expected during the next decades for the air traffic [1]. Already today, the aviation sector accounts for around 11% of the energy consumption of the entire transport sector [2] and thus contributes significantly to the global greenhouse gas emissions. Even under consideration of further technology developments and efficiency improvements, the aviation sector could emit three times the current amount of CO_2 by 2050 if no actions are taken [3]. Although the aviation sector is comparatively seen as the most difficult to decarbonize as there is no feasible short-term possibility for aircraft electrification [3], sustainable aviation fuels (SAF) based on biogenic raw materials and renewable energy represent an option to significantly decrease the emissions of the aviation sector. However, SAF currently accounts for only about 0.1% of the total kerosene consumption [2].

Despite the fact that the vast majority of current SAF is represented by biofuels [4], kerosene produced via the Power-to-Liquid (PtL) process based on renewable electrical energy offers a viable option for a future sustainable aviation fuel supply [5].

1.2. Related studies

There are various studies addressing the topic of SAF with a focus on biofuels (e.g. [6-9]). Mawhood et al. [6] present possible production routes and evaluate the related

 doi:10.20944/preprints202101.0564.v1

technologies based on their future potentials. The role of the Fischer-Tropsch (FT) synthesis as part of biofuel production is presented by Ail & Dasappa [7], considering literature data from FT processes under operation. Hamelinck et al. [10] developed a process model based on Aspen Plus® for the technical and economical evaluation of a Biomass-to-Liquid (BtL) process. Similar studies were performed by Sudiro & Bertucco [11] and Lee et al. [12], providing simulation models for different production routes based on Aspen Plus® with a main focus on gasoline and diesel.

Schmidt et al. [5] introduced the PtL process as a relevant option for aviation fuel production and provided techno-economic and environmental comparisons between different process routes based on literature data. An extensive simulation model for a PtL process was developed by König et al. [13] with Aspen Plus® providing conclusions regarding the process internal correlations and overall efficiencies. Studies concerning the decentralization of FT-based fuel production are carried out by Kirsch et al. [14] providing insights on the current state of technology development by the Institute for Micro Process Engineering of Karlsruhe Institute of Technology and the INERATEC GmbH. The work presented here is an extension of a conference paper [15].

1.3. Novelty

The novelty of this work is the description of a process chain tailored to a decentralized and sustainable production of kerosene which can be used directly on site for an exemplary application. In the case of Brazil, the current highly centralized production of kerosene [16] in conjunction with the huge state territory leads to long transportation routes across many state borders and therefore results in high kerosene prices for remote airports. A decentralized production of kerosene on site might therefore already be cost competitive and thus represent a viable option as early stage application field.

This paper also describes the development of a Fischer-Tropsch reactor model as part of a future open source process simulation model based on Python, showing the importance of the FT reactor as core of the PtL process. The purpose of the modular python-based process model framework is to support the trend towards open and linkable integrated models and to facilitate the system analytical assessment of different fuel production pathways by enabling the possibility of a direct coupling with energy system or scenario assessment models. It further will ease multi-criteria assessment and optimization in conjunction with e.g. open life-cycle-assessment tools. The targeted technical level of detail is therefore lower than that made possible by commercial software as e.g. Aspen Plus®, but enables a sufficient representation of process related main degrees of freedom.

1.4. Summary

Under consideration of general assumptions regarding future synthetic fuel certification, various possibilities for the synthetic generation of kerosene are qualitatively compared and the most suitable production pathway for a decentralized application in remote areas is determined as the PtL process. The process route is examined subdivided into its three main sections, namely synthesis gas generation, synthetic crude production and crude refining, considering current technologies. For each main process step, the currently relevant technical possibilities are described and specific technologies fitted to the desired product, the decentralized application and the entire process chain are determined, showing that a process including a synthesis via FT reaction is the most advantageous.

For demonstration of the influence of the Fischer-Tropsch reactor as key of the process, the development of the Python-based reactor model is described. The impacts of the main process parameters are shown by means of the model and resulting effects on up- and downstream processes are pointed out, showing the reactor temperature to be the most prominent operation parameter for a targeted syncrude composition and thus the decisive character of the reactor.

2. Materials and Methods

 doi:10.20944/preprints202101.0564.v1

2.1. Assumptions and limitations

At the present time the technical specifications to be met of the main fuel types used in civil aviation - Jet A and Jet A-1, are defined by the international standards ASTM D1655 [17] and DEF STAN 91-91 [18]. The consideration of SAF and definition of its requirements is regulated by annexes of the ASTM D7566 [19], providing various approved production pathways. One of the seven currently approved production routes describes a Synthetic Paraffinic Kerosene (SPK) via Fischer-Tropsch reaction (FT-SPK) [19]. To be certified as a drop-in fuel according ASTM D7566, the FT-SPK may only be used as a blend to conventional jet fuel from crude oil with a maximum blending ratio of up to 50%. Currently, even among the other certified production routes, there is no short-term possibility for the production of a certified Jet A or Jet A-1 with a sustainable kerosene share of more than 50%.

As one of the main drivers behind the idea of sustainable decentralized kerosene production is the avoidance of long-distance transport of fuel from the refinery to the consumer, two main assumptions are made regarding the background of the general idea of the presented application.

2.1.1. Certification of 100% FT-SPK

This study treats the use of 100% FT-SPK as near-drop-in fuel. The underlying assumption is, that the use of 100% FT-SPK will be certified for the use in slightly modified aircrafts (e.g. compatible sealings [20, 21]). In contrast, drop-in fuels have to be compatible with the whole legacy fleet.

2.1.2. Quality testing

The second main assumption is made regarding the jet fuel quality testing process itself. Currently, every batch produced must pass a series of quality tests in certified laboratories before it can be released for use as fuel for the civil aviation [17, 22]. A decentralized production, especially in remote regions of comparatively small quantities would - if this test procedure were to be maintained at the same level - involve immense logistical and financial expenses and might not be sustainable and feasible. Accordingly, it is assumed that adapted regulations and procedures will be developed for a sustainable decentralized kerosene production in the future, which will enable a certified quality testing on site.

2.2. Production route

The production of alternative fuels is possible through many different process routes which can be categorized in different ways. One type of categorization is based on the underlying feedstock, subdividing them into the Biomass-to-Liquid process - covering the production of “biofuels” based on biogenic raw materials of different types and the Power-to-Liquid process, shown in Figure 1, which describes a synthetic production based solely on electrical energy as energy input - providing “e-fuels”. These variants can be supplemented by two further minor options, a mix of both previous types, the Power-Biomass-to-Liquid (PBtL) and the technology defined as Sun-to-Liquid process (StL) which uses sunlight for the direct production of synthesis gas either in a photo-electrochemical cell or via a thermochemical reactor [23].

Even though the latter StL technology path may be an interesting option in the future, it will not be considered in the further course of the work as it is still in the stage of development [24, 25].

Preprints (www.preprints.org) | NOT PEER-REVIEWED | Posted: 27 January 2021 doi:10.20944/preprints202101.0564.v1

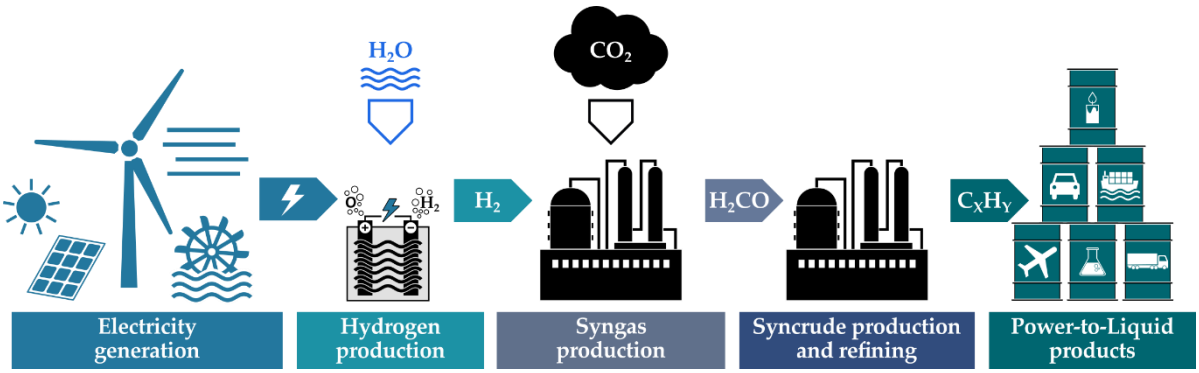

Figure 1. Generic scheme of a Power-to-Liquid process

For a classification of the other above-mentioned production routes with regard to their suitability for a decentralized and sustainable application, it is necessary to evaluate the role of the required process-specific feedstocks in particular.

2.2.1. Feedstock availability

A decentralization of kerosene production as presented in this work not only means the final products decoupling of central generation and transport structures, but as well the localization of the upstream raw material and educts supply. Since there is no possibility to compensate for product overcapacities or bottlenecks via connected infrastructure, on-site matching between demand and supply is crucial. For operational and economic reasons, it is still relevant to avoid unnecessary oversizing of the plant and to strive for the most constant plant operation possible. As a result, a constant supply of raw materials is necessary. If one compares the two mentioned production categories in this respect, there are clear advantages for the variant of an electrical energy supply for the following reasons. For a sustainable use of biomass, it must be ensured that only residues from other biomass processing sectors are used or that targeted fuel-related biomass production meets the requirements of current sustainability criteria [26-29].

In the case of a remote application, the probability that an industry will have usable biomass available as a by-product or residue produced in a consistent quality and sufficient quantity is low, even without considering the necessity of year-round availability.

Electrical energy as feedstock offers greater flexibility in this respect, as it is not dependent on local structures or the raw material supply of third parties. Decentralized electrical energy generation using a mix of photovoltaics, wind and water power tailored to the location, its energy potentials and the plants demand can provide the required energy. Short-term fluctuations can be compensated via electrical energy storages or by buffering them through a hydrogen storage within the process.

2.2.2. Local impacts

In order to evaluate the above-mentioned possibility of using certified biomass as raw material, main local environmental influences are compared in the following. The key aspects to consider here are the specific water and land demand related to the amount of fuel produced. Both the water and land demand of biomass-based fuels are highly dependent on the specific type of feedstock and vary between approximately 500 to 20,000 l_{water}/l_{fuel} and 0.85 to 17.3 $m^2/l_{fuel}/y$ respectively. The comparison with the parameters of a PtL production which result in a water demand of up to 1.38 l_{water}/l_{fuel} and a land demand between 0.33 and 0.74 $m^2/l_{fuel}/y$ [25] (varying due to the type of energy production), shows the local disadvantages of a production based on primary biomass.

To summarize – under certain conditions, especially if usable biogenic residues are available as raw material in sufficient consistency, quality and quantity or there are potentials for sustainable use of primary biomass, the use of a BtL process is reasonable. However, as this cannot be presupposed for the decentralized application under consideration here, PtL is clearly defined as the preferred process route and will be examined subsequently.

Preprints (www.preprints.org) | NOT PEER-REVIEWED | Posted: 27 January 2021 doi:10.20944/preprints202101.0564.v1

2.3. Process design

The simplified process design outlined in the following section is based on the idea of a design with a clear focus on the final on-specification product kerosene considering the above production route selection and requirements, in particular the avoidance of biogenic raw materials and the exclusive use of renewable electrical energy as external energy source. An exemplary flow sheet of the simplified resulting process setup following [13] is shown in Figure 2.

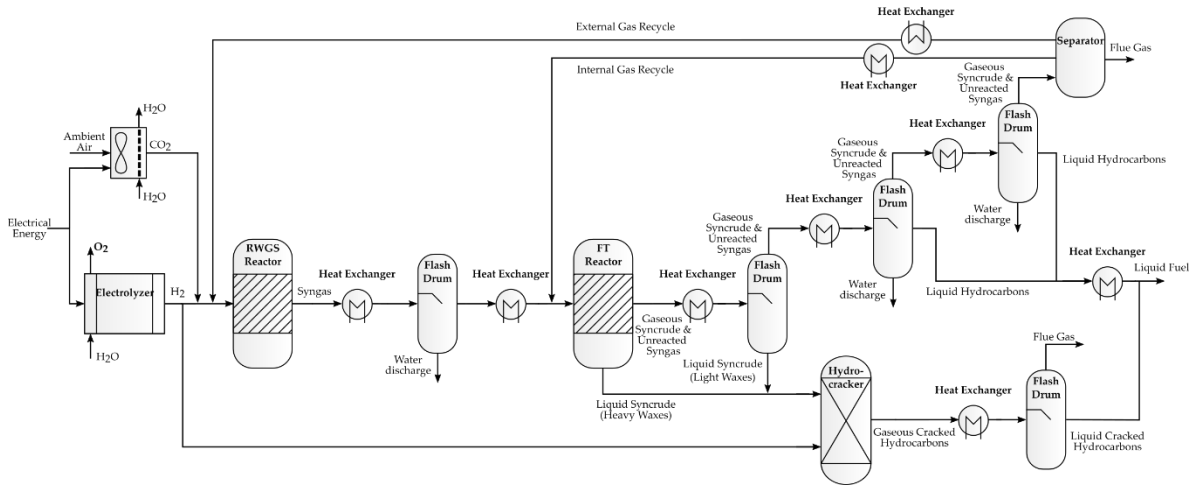

Figure 2. Simplified process flow sheet of a possible Power-to-Liquid process for a decentralized application with a focus on kerosene as main product.

In order to decide on a specific production route, the suitability of the various possible PtL routes for decentralized application are considered. As part of this category, currently there are mainly two relevant options for the production of liquid hydrocarbons in kerosene range – the production via methanol synthesis, also described as Alcohol-to-Jet (AtJ) and the production via Fischer-Tropsch synthesis. The main difference between the two catalytic synthesis types lies in the synthesis reaction itself and the processing of the intermediate to the final product. While the properties of the corresponding fractions of the intermediate product already approximately comply with the required specifications when using FT-synthesis [30], the methanol synthesis requires a rather complex product preparation which involves various processing steps. A possible third option complementing the category of AtJ, the ethanol synthesis, which currently plays a minor role as it is still in an early stage of development, comes with the same disadvantages of high refining effort.

In order to achieve a simple plant design with minimum complexity, PtL via FT-synthesis is therefore the most suitable option.

The synthetic fuel production based on a Fischer-Tropsch reactor can mainly be separated into three sections – (I) the generation of synthesis gas (syngas), (II) the generation of synthetic crude (syncrude) via FT-synthesis and (III) a subsequent separation, upgrading and/or refining of the syncrude to the intermediate or final product [30]. The process chain is described in the following based on this subdivision.

2.4. Syngas generation (I)

The composition of the syngas as feed for the FT-reactor has a significant impact on the synthesis process and is therefore largely determined by the desired effects and outputs of this process. Since the desired final product is a mixture of hydrocarbons the syngas required for a FT process shall mainly consist of the reactants hydrogen (H_2) and carbon monoxide (CO).

The various available options for synthesis gas production can be divided into the direct syngas production, covering the simultaneous production of both reactants based

Preprints (www.preprints.org) | NOT PEER-REVIEWED | Posted: 27 January 2021 doi:10.20944/preprints202101.0564.v1

on a single feedstock and the indirect syngas production which describes the separate production of the main syngas components, with either the same or different types of feedstock. A direct syngas generation is currently only possible by using bio routes or the StL process. Since biogenic materials or by-products like glycerol are not considered further as raw material in this paper according the above description, the focus in the subsequent sections will be placed on the indirect syngas production.

2.4.1. Hydrogen production

For the production of hydrogen, the electrochemical process of water electrolysis is used, which splits water into hydrogen and oxygen (1) under electric voltage.

$$H_2O \rightarrow H_2 + \frac{1}{2}O_2 \quad (1)$$

As of today, there are three main technologies that can be applied. The proton exchange membrane (PEM) and alkaline electrolysis (AEL), both of which have long been used commercially and are technically highly developed, and the solid oxide electrolysis cell (SOEC) as a still very recent technology [31].

Even if the PEM and AEL can score with a proven technology and relatively low specific investment costs, the SOEC comes with some notable advantages. Unlike the others, it is operated with hot steam and not with liquid water, which is why it is alternatively called high temperature electrolysis (HTE). This leads to high electrical efficiencies that already exceed those of the other established technologies by more than 10% [31]. A precondition for operation at the required high temperatures of more than 650 °C is a sufficient heat supply. Since the FT-reaction is highly exothermic [30], the SOEC is particularly suitable, as the reactors waste heat can be used process internally as heat source for the hot steam generation. An additional improvement of the SOEC is provided by current research activities, which aim at a further development of the co-electrolysis (co-SOEC) providing syngas directly from water, CO_2 and electrical energy (2).

$$H_2O + CO_2 \rightarrow H_2 + CO + O_2 \quad (2)$$

A first small-scale unit of this type has already gone into operation [32].

2.4.2. CO production

Given that the extraction of carbon monoxide on the basis of industrial residues is excluded for decentralized application, a detour via carbon dioxide has to be taken, as CO does not occur naturally accessible in the surrounding. Therefore, a carbon capture and utilization (CCU) technology can be applied in which CO_2 is extracted from the ambient air via direct air capture (DAC). Even though different DAC absorption technologies are already under investigation and in application since several decades, it's the adsorption processes that are becoming increasingly important for CO_2 capture due to their lower specific energy consumption [33]. As one of the possible adsorption types, the temperature-vacuum swing adsorption (TVS) represents a technology that is already in commercial use [34] and qualifies in particular for a decentralized PtL process. As with the SOEC, both electrical and thermal energy must be provided for the operation of a TVS-DAC. The comparatively low required temperature of below 100 °C [35] can also be decoupled from the exothermal synthesis process.

If the above-mentioned co-SOEC is not applied in order to use CO_2 directly for the synthesis gas production, the conversion of the CO_2 into CO must be carried out in a further process step, the reverse water-gas shift reaction (rWGS).

The rWGS describes the hydrogenation of CO_2 into CO and H_2O (3).

$$CO_2 + H_2 \leftrightarrow CO + H_2O \qquad \Delta H^0_{298K} = +41\ kJ/mol \quad (3)$$

Since the reactivity of CO_2 is lower than that of CO, the chemical equilibrium is on the side of the reactants [36]. A shift of the equilibrium of the endothermic reaction can be obtained by an increase of the reaction temperature. To avoid undesirable side reactions like methanation and the Sabatier reaction, leading to the formation of Methane (CH_4),

Preprints (www.preprints.org) | NOT PEER-REVIEWED | Posted: 27 January 2021 doi:10.20944/preprints202101.0564.v1

reaction temperatures above 700 °C are necessary; to prevent the formation of soot, temperatures above 800 °C should be even targeted at standard conditions [37]. Enhancements of the CO_2-conversion and the reduction of the necessary reaction temperature and probability of side reactions can be further achieved by an altered pressure, adaption of the input gas shares or the integration of catalysts [38].

2.5. Syncrude generation (II)

The production of syncrude by the FT synthesis represents the core of the process, as it is decisive for both the syngas composition and therewith the upstream process steps as well as the syncrude composition and therewith the upgrading requirements – the downstream processes. The FT synthesis refers to a process synthesizing a gas to a synthetic crude oil – the syncrude, composed of a wide range of hydrocarbon chains of different lengths [30]. For a main classification, the reaction is categorized according to the temperature and catalyst type into iron-based high-temperature FT (Fe-HTFT), iron-based low-temperature FT (Fe-LTFT) and cobalt-based low-temperature FT (Co-LTFT). The main effect of the different temperature level is a shift in the average syncrude chain lengths. HTFT, due to an increased hydrogenation rate and desorption activity from the catalyst surface, mainly aims shorter carbon chains $<C_{10}$, whereas LTFT mainly leads to longer carbon chains $>C_{10}$ (mass %) [30]. The major impact of the choice of the catalyst material concerns the share of the syncrude compound classes, which get primarily represented by paraffins (alkanes), olefins (alkenes), aromatics and oxygenates. With regard to longer-chain hydrocarbons, cobalt-based catalysts lead almost exclusively to the formation of paraffins, whereas with iron-based catalysts both olefins and oxygenates are formed in notable proportions. The formation of aromatics is only promoted in the case of Fe-HTFT for some chain length ranges [30].

Since olefins have a deleterious effect on the fuel stability and the proportion of oxygenates should be reduced to a minimum to avoid gum formation [39], a Co-LTFT reactor is selected as appropriate synthesis process step for this study, as well under consideration of a reduced necessary refining effort. The corresponding mainly occurring chemical reaction equations for the synthesis are:

$$\text{Paraffins: } nCO + (2n+1)H_2 \rightarrow H_2(CH_2)_n + nH_2O \quad (4)$$

$$\text{Olefins: } nCO + 2nH_2 \rightarrow (CH_2)_n + nH_2O \quad (5)$$

2.6. Separation, upgrading and refining (III)

The LTFT process provides a syncrude with a temperature around 200 °C, whereby a stepwise subsequent cooling with a cascaded sequence of flash drums is appropriate for syncrude fractionation. Since the production of syncrude via a FT reactor comes with a broad spectrum of hydrocarbon chains of varying lengths and only the small fraction between C_8 and C_{16} is relevant for conventional jet fuel [40], there are always by-products which cannot contribute to the main product. In optimized refineries, those by-products usually get upgraded or refined to shift them into another chain length range or to provide a set of various final products [39]. This increases the overall plant efficiency significantly. Nevertheless, for a decentralized demand-driven production of kerosene, the focus lies on the main product and thus no extensive refining for further products is carried out in this study. Hydrocracking is considered as the only refining step, focusing on an easily achievable kerosene yield with low process complexity.

2.6.1. Hydrocracking

One objective of a hydrocracking unit in a FT process is to crack heavy long-chain hydrocarbons above the kerosene range into lighter short-chain hydrocarbons and to remove heteroatoms by saturating the compounds via hydrogenation to obtain a paraffinic product [41]. Under the presence of a catalytic material - for FT feed usually based on

Preprints (www.preprints.org) | NOT PEER-REVIEWED | Posted: 27 January 2021 doi:10.20944/preprints202101.0564.v1

palladium or platinum – the syncrude is mixed with hydrogen in the hydrocracking unit at around 360 °C [41]. In terms of the desired fuel properties, the resulting cracked hydrocarbon chains benefit from a further effect which takes place during the hydrocracking. The FT syncrude consists mainly of linear paraffins with a relatively high freezing point, the hydrocracked output on the other hand shows a significant increase of branched isoparaffins [42], which are necessary to meet the low freezing points of -47 °C for Jet A-1 [18] defined by the specification - respectively -40 °C for Jet A [17].

Although still in the development stage and therefore not considered in the process outlined in this paper, the integration of hydrocracking in the FT reactor may in future offer a further opportunity to reduce plant complexity and enhance the process efficiency [14].

2.7. Process recycles

In addition to the main system components, the process-internal gas recycles play an important role for the process efficiency, as unconverted syngas is recycled after the product separation and fed back into the process, which is described as closed gas loop [30]. The closed gas loop can include an internal recycle, defined here as the recirculation of the tail gases into the syngas in front of the FT reactor and an external recycle describing the recirculation to an earlier process step, for example the rWGS reactor.

2.8. Reactor modelling of Fischer-Tropsch

To assess and evaluate the influence of the FT reactor on up- and downstream processes, a kinetic Python model of a cobalt-based LTFT reactor was developed based on current literature.

2.8.1. Components and physical correlations

In order to take the wide product range of a FT syncrude into account, n-paraffins from C_1H_4 to $C_{45}H_{92}$ and olefins from C_2H_4 to $C_{45}H_{90}$ are considered in addition to the main components H_2, CO, H_2O, and CO_2. Thermophysical properties of paraffins and olefins are based on [43]. For simplification, it is assumed that the saturated hydrocarbons of the FT syncrude consist only of linear paraffins. For olefins, mean values of linear compounds and isomers with single branching were calculated.

For the chemical components real gas behavior is taken into account and physical behavior is calculated according Peng-Robinson equation of state (PREOS) [44].

2.8.2. Carbon number distribution

The carbon number distribution, which describes the proportions of the individual chain lengths in the product spectrum, is calculated with the Anderson-Schulz-Flory (ASF) distribution [45] according equation (6). It sets the product molar fraction M_n of an individual chain length n in relation to the chain growth probability α (CGP), the value that describes the probability that chain propagation occurs as opposed to chain termination.

$$M_n = \alpha^{(n-1)}(1-\alpha) \tag{6}$$

The calculation of α is performed by equation (7) according [46]:

$$\alpha = \frac{1}{1 + k_a \left(\frac{c_{H_2}}{c_{CO}}\right)^{\beta} exp\left(\frac{\Delta E_{a,\alpha}}{R}\left(\frac{1}{493.15} - \frac{1}{T}\right)\right)} \tag{7}$$

with k_a as quotient of rate constants for chain growth termination and propagation, c_x as molar concentration of species x (H_2 and CO), β as syngas ratio power constant, $\Delta E_{a,\alpha}$ as difference in activation energy for the termination and propagation reactions of the chain growth mechanism [46], R as universal gas constant and T as temperature. The corresponding values are shown in Table 1.

Preprints (www.preprints.org) | NOT PEER-REVIEWED | Posted: 27 January 2021 doi:10.20944/preprints202101.0564.v1

This definition of α creates a dependency of the growth probability on reactor temperature and on syngas composition.

To account for the formation of olefins, which affects primarily the shorter product fractions, a chain length dependent paraffin to olefin ratio is calculated according [47] with:

$$\frac{M_{Olefin}}{M_{Paraffin}} = \exp(-d) \tag{8}$$

where constant d = 0.3.

Table 1. Kinetic parameter values for the calculation of CGP and reaction rates

Parameter	Value	Unit
	CGP [46]	
k_a	0.0567	-
β	1.76	-
$\Delta E_{a,\alpha}$	120.4 x 10^3	J/mol
	Reaction rate methane [48]	
a_{CH_4}	-0.86	-
b_{CH_4}	1.32	-
q_{CH_4}	0.46	-
k_{0,CH_4}	2.925 x 10^{-7}	mol/g/s/MPa$^{(a+b)}$
E_{a,CH_4}	136 x 10^3	J/mol
	Reaction rate FT [49]	
a_{FT}	-0.31	-
b_{FT}	0.88	-
q_{FT}	-0.24	-
$k_{0,FT}$	3.694 x 10^{-6}	mol/g/s/MPa$^{(a+b)}$
$E_{a,FT}$	104 x 10^3	J/mol

2.8.3. Reaction rates

The reaction rate equations and kinetic parameters are based on the work of [48, 49]. For reasons as yet unknown in detail, the FT reaction does not fully follow the ASF distribution but shows some deviations for certain chain lengths, especially a significant increase of C_1 and a minor decrease of C_2 selectivity [30]. As for simplification, the decrease of C_2H_6 and C_2H_4 selectivity will not be considered.

The increased fraction of CH_4 is taken into account by reaction rate equation (9) based on [48] with parameter values according Table 1:

$$r_{CH_4} = \frac{k_{CH_4} {p_{CO}}^{a_{CH_4}} {p_{H_2}}^{b_{CH_4}}}{\left(1 + q_{CH_4} \frac{p_{H_2O}}{p_{H_2}}\right)^2} \tag{9}$$

with r_{CH_4} as methane reaction rate (mol/s/g), a_{CH_4} and b_{CH_4} as reaction orders of the partial pressures p for CO and H_2 and q_{CH_4} as water effect constant for CH_4 formation.

The temperature dependent reaction rate constant k_{CH4} is defined as:

$$k_{CH_4} = k_{0,CH_4} exp\left(\frac{E_{a,CH_4}}{R}\left(\frac{1}{493.15} - \frac{1}{T}\right)\right) \tag{10}$$

where k_{0,CH_4} describes the reaction rate constant at 493.15 K and E_{a,CH_4} the activation energy for CH_4 formation [48]. The special feature of this equation compared to other kinetic

Preprints (www.preprints.org) | NOT PEER-REVIEWED | Posted: 27 January 2021 doi:10.20944/preprints202101.0564.v1

datasets available in current literature is the consideration of the influence of water which is one main by-product of the process and may as well be present in the syngas feed.

For the further product spectrum, the reaction rate is defined based on [49] by the equation:

$$r_{FT} = \frac{k_{FT} {p_{CO}}^{a_{FT}} {p_{H_2}}^{b_{FT}}}{\left(1 + q_{FT} \frac{p_{H_2O}}{p_{H_2}}\right)} \tag{11}$$

with r_{FT} as FT reaction rate, k_{FT} as temperature dependent reaction rate constant calculated via:

$$k_{FT} = k_{0,FT} \exp\left(\frac{E_{a,FT}}{R}\left(\frac{1}{493.15} - \frac{1}{T}\right)\right) \tag{12}$$

where $k_{0,FT}$ is the reaction rate constant at 493.15 K and $E_{a,FT}$ the activation energy. Both reaction rates presented above refer to the molar amount of reacted CO molecules.

The chain length specific reaction rates $r_{i,n}$ for all considered chain lengths n and $i \in$ paraffin $\wedge$ olefin for all following equations are calculated via:

$$r_{i,n} = \frac{M_{i,n} m_{mol,i,n}}{\sum_{n=1}^{45} M_{i,n} m_{mol,i,n}} r_{FT} \tag{13}$$

with m_{mol} as molar mass (g/mol) where - to account for the methane deviation – all $r_{i,n}$ for n >1 are multiplied with the FT methane reaction rate according (14) and $r_{i,n}$ is substituted for i = paraffin and n = 1 (15):

$$r_{i,n} = r_{i,n}\left(1 + \frac{r_{paraffin,1}}{r_{FT}}\right) \tag{14}$$

$$r_{paraffin,1} = r_{CH_4} \tag{15}$$

A normalized dimensionless selectivity S is introduced (16), which is used to redefine the specific reaction rates (17) and thus meet the reaction rate r_{FT} of the total synthesis process:

$$S_{i,n} = \frac{r_{i,n}}{\sum_{n=1}^{45} r_{i,n}} \tag{16}$$

$$r_{i,n} = S_{i,n} r_{FT} \tag{17}$$

2.8.4. Partial pressures

The partial pressures of the relevant components which form the basis for the above reaction rate equations (9) and (11) are calculated based on the H_2 usage ratio ur_{H_2} and the reaction rates, showing the iterative character of the reactor calculation.

The resulting pressures are either calculated as mean values between the partial pressures at the reactor outlet after the reaction and the reactor inlet for reactor types with a plug flow reactor characteristic (PFR) or calculated based entirely on the product composition at the reactor outlet according equations (18) - (20) for reactor types that can be classified as a continuous stirred-tank reactor (CSTR):

$$p_{H_2,out} = p\left(\frac{c_{H_2,in}\dot{N}_{total} - 2m_{cat} ur_{H_2} \sum_{n=1}^{45} r_{i,n}}{\dot{N}_{total}}\right) \tag{18}$$

$$p_{CO,out} = p\left(\frac{c_{CO,in}\dot{N}_{total} - 2m_{cat} \sum_{n=1}^{45} r_{i,n}}{\dot{N}_{total}}\right) \tag{19}$$

$$p_{H_2O,out} = p\left(\frac{c_{H_2O,in}\dot{N}_{total} + 3m_{cat} \sum_{n=1}^{45} r_{i,n}}{\dot{N}_{total}}\right) \tag{20}$$

Preprints (www.preprints.org) | NOT PEER-REVIEWED | Posted: 27 January 2021 doi:10.20944/preprints202101.0564.v1

with $\dot{N}_{total}$ as syngas particle flow (mol/s) and m_{cat} as reactor catalyst mass (g).

2.8.5. H_2 usage ratio

The H_2 usage ratio describes the ratio between converted H_2 and converted CO during the FT reaction. The specific proportion of $ur_{H_2 i,n}$ varies for each paraffin of different length according equation (4) between 2 and 3. The H_2 usage ratio for olefins equals 2 over the whole product range as per equation (5). The average H_2 usage ratio of the entire product spectrum is therewith calculated based on the component type and chain length specific reaction rate shares:

$$ur_{H_2} = \sum_{n_1=1}^{45} \frac{r_{i_1,n_1}}{\sum_{n_2=1}^{45} r_{i_2,n_2}} ur_{H_2 i_1,n_1} \tag{21}$$

2.8.6. CO conversion

The CO conversion u_{CO} as one key parameter of the reactor operation is calculated inter alia based on the above described reaction rates and the gas hourly space velocity (GHSV) which indicates the hourly syngas flow rate per gram of catalyst loading:

$$u_{CO} = \frac{2 \frac{\dot{V}_{total}}{GHSV} \sum_{n=1}^{45} r_{i,n}}{c_{CO,in} \dot{N}_{total}} \tag{22}$$

with $\dot{V}_{total}$ as volumetric syngas flow (NL/h).

2.8.7. Calculation method

Figure 3 demonstrates the simplified calculation flow sheet which is based on the equations presented above. The interdependencies between the partial pressures, the reaction rates and the H_2 usage ratio lead to an iterative calculation which is performed until the specific deviation for the CO conversion and H_2 usage ratio is below 0.001%. The predefined input compound which is fed to the reactor as syngas is defined in particular by the shares of its components–providing the necessary molar concentrations of H_2, CO and H_2O–its temperature, pressure and flow rate.

2.9. Model validation

A comparison of experimental [48, 49] and modeled reaction rates, showing the expected reactor behavior and leading to satisfactory coefficients of determination is shown in Appendix B.

For a further evaluation of the model validity with regard to the intended model purpose of representing the possible degrees of freedom by means of conclusive parameter correlations, the main dependencies between the adjustment of key reactor parameters

Preprints (www.preprints.org) | NOT PEER-REVIEWED | Posted: 27 January 2021 doi:10.20944/preprints202101.0564.v1

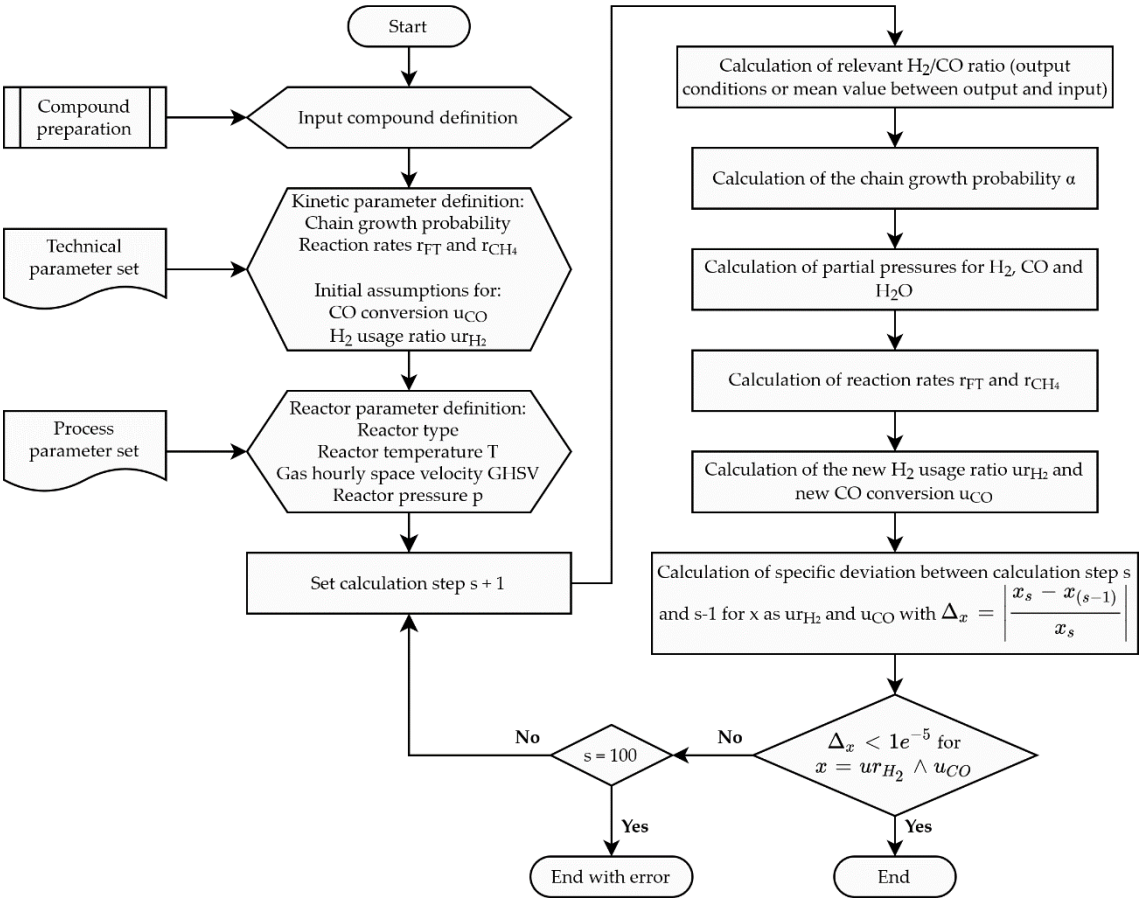

Figure 3. Flow chart of the FT reactor calculation model

and the reactor behavior are examined. The main correlations for cobalt-based FT-reaction in consideration of the model simplifications made are shown in Table 2.

Table 2. Dependencies of the reactor behavior on the main Fischer-Tropsch reactor operation parameters [30, 46, 50, 51] for cobalt-based catalysts.

	Operation parameters:			
	▲ Temperature	**▲ Pressure**	**▲ GHSV**	**▲ H_2/CO ratio**
Reactor behavior:				
CGP	▼	•	•	▼
CH_4 selectivity	▲	▼	▲	▲
Syngas conversion	▲	▲	▼	○

▲ = increase, ▼ = decrease, • = minor impact, ○ = more complex dependency

The presented correlations are shared by a majority of the available literature concerning the cobalt-based FT reaction. Some variations can be found regarding the impact of a pressure increase on the chain growth potential and the effect of a change in GHSV on the CH_4 selectivity. While [30] concludes a rising CGP with an increase of the reactor pressure other studies tend to conclude that the pressure impact on the CGP is negligible [46, 50]. A decrease of methane selectivity resulting of an increase in GHSV which is concluded by [30] is opposed to an increase of CH_4 selectivity [48, 51] for cobalt-based catalysts at typical FT operation parameter ranges, which can be attributed to the influence of the by-product water which suppresses methane formation [48, 51] and which share is increased at elevated syngas conversion rates. One reason for the varying dependencies in different sources can be the significant influence of the catalyst material on the reactor behavior

Preprints (www.preprints.org) | NOT PEER-REVIEWED | Posted: 27 January 2021 doi:10.20944/preprints202101.0564.v1

thus in the following, the dependencies which clearly address cobalt-based catalysts are assessed for the model validation.

Figure 4 shows the effects on the reactor for a varying temperature (a) and pressure (b) based on the reactor model. The expected reactor behavior is well represented by the model results. The same applies for the impact of the GHSV (c) and the syngas reactants ratio (d).

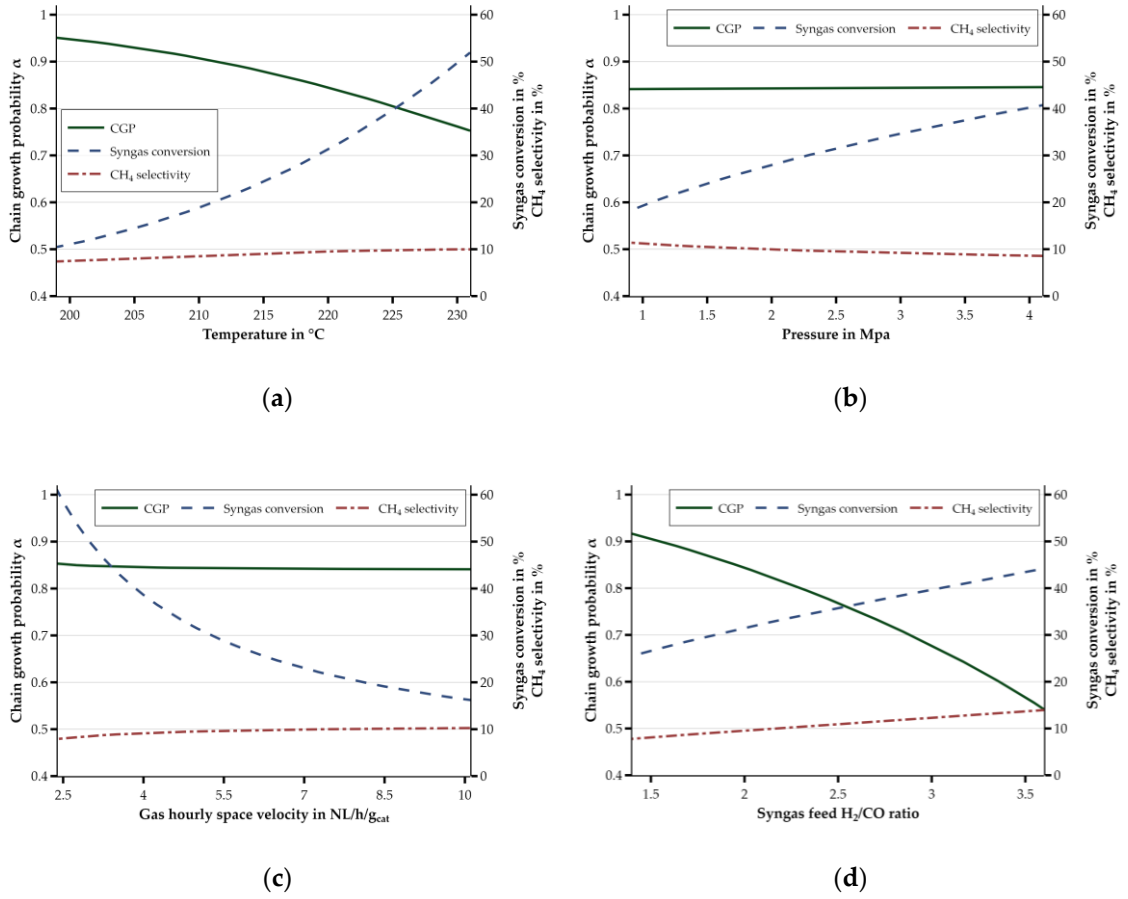

Figure 4. Key parameters of the FT reactor calculated on the basis of the model showing **(a)** the temperature-dependency for a fixed-bed-reactor with p = 2.5 MPa, GHSV = 5 NL/h/gcat, H2/CO syngas feed ratio = 2, **(b)** the pressure-dependency for a fixed bed reactor with T = 220 °C, GHSV = 5 NL/h/gcat and H2/CO syngas feed ratio = 2, **(c)** the dependency from the GHSV for a fixed-bed-reactor with T = 220 °C, p = 2.5 MPa, H2/CO syngas feed ratio = 2 and **(d)** the dependency on the H2/CO syngas feed ratio for a fixed bed reactor with T = 220 °C, p = 2.5 MPa and GHSV = 5 NL/h/gcat.

3. Results and discussion

To show the relevance of the FT reactor and its operation parameters as part of a PtL process regarding the following downstream and previous upstream processes, a closer look at the resulting syncrude composition is necessary. Figure 5 visualizes the impacts of a pressure adjustment (a) and an increase of the GHSV (b) on the converted syngas, showing the selectivity and its share of hydrocarbon chains with a chain length between C_8 and C_{16} representing the compounds which are considered part of kerosene. Additionally, the shares for shorter hydrocarbon chain length ranges C_{7-} and longer ranges C_{17+} are provided. As can be expected from Figure 4 (b) and (c) due to the insignificant impact on the CGP, adjustments of those two operation parameters only show minor effects on the syncrude composition. The biggest impacts concerning the reactor reactivity resulting at elevated pressures and the decrease of syngas conversion with increased GHSV mainly address the basic plant design in terms of size and structure. Thus, they are not parameters

Preprints (www.preprints.org) | NOT PEER-REVIEWED | Posted: 27 January 2021 doi:10.20944/preprints202101.0564.v1

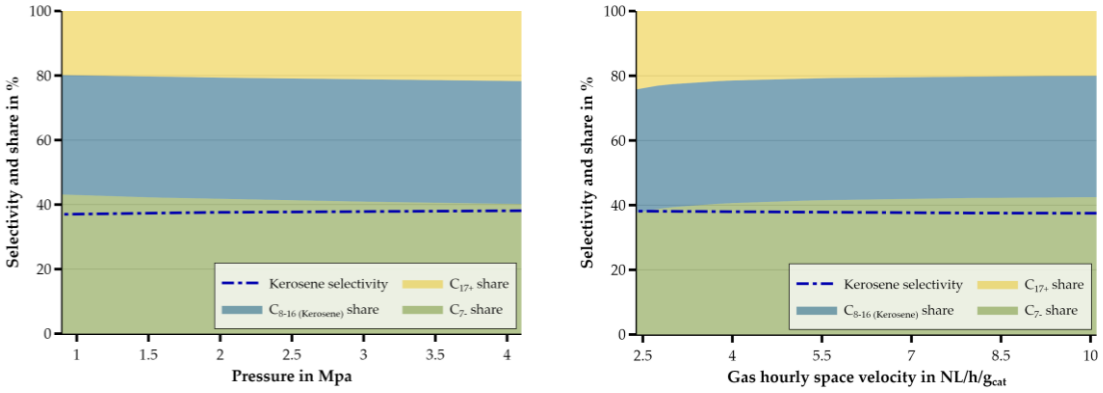

(a) (b)

Figure 5. Reactor selectivity shares of different carbon chain length ranges and the kerosene range selectivity on the basis of the model showing **(a)** the pressure-dependency for a fixed bed reactor with T = 220 °C, GHSV = 5 NL/h/gcat and H2/CO syngas feed ratio = 2 and **(b)** the dependency from the GHSV for a fixed-bed-reactor with T = 220 °C, p = 2.5 MPa, H2/CO syngas feed ratio = 2.

governing the surrounding process steps, but are part of an overarching dimensioning and plant optimization, in particular with regard to deactivation and lifetime of the reactor catalyst load [52].

The effects of a variation of the reactor temperature are provided Figure 6, showing a strong influence on the syncrude distribution. The decreasing probability of chain growth caused by an increase of the temperature according Figure 5 (a) leads to high shares of light short-chained hydrocarbons at elevated temperatures. The selectivity maximum for hydrocarbons within the kerosene chain length range can be found at around 220 °C with close to 38%, but although the focus of this work and the process under consideration is on kerosene as main product, maximizing the straight run kerosene output of the reactor may not be expedient in consideration of the overall process efficiency. As the refining of the syncrude is crucial to meet relevant fuel specifications which is why a hydrocracking unit is selected as part of the process, the aim should be to maximize the

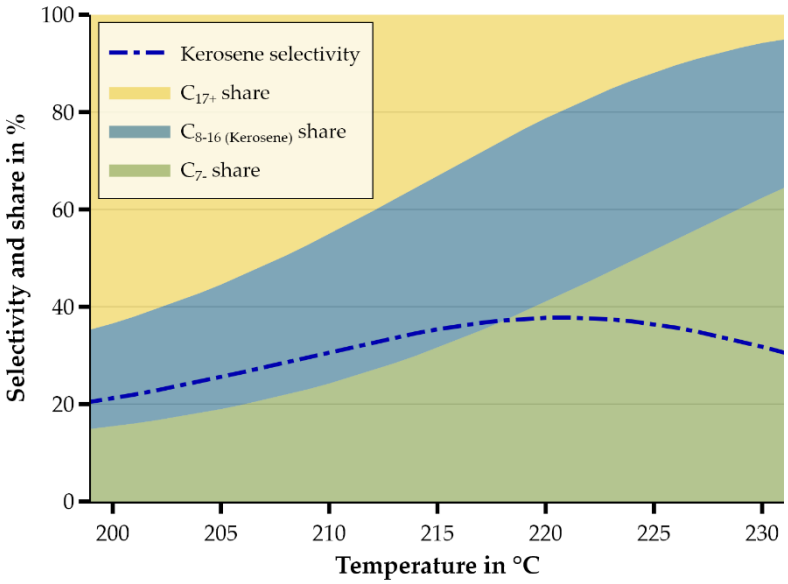

Figure 6. Temperature dependency on selectivity shares and kerosene range selectivity for a fixed bed reactor with p = 2.5 MPa, GHSV = 5 NL/h/g_{cat} and H_2/CO syngas feed ratio = 2.

Preprints (www.preprints.org) | NOT PEER-REVIEWED | Posted: 27 January 2021 doi:10.20944/preprints202101.0564.v1

share of syncrude fractions, which can further be refined to on-specification products. In the case of a synthesis with a subsequent hydrocracker where long-chained hydrocarbons can be cracked into kerosene range, optimizing the yield of hydrocarbons with a chain length above C_8 might be beneficial. However, certain reactor conditions that would lead to unwanted side effects like an increased reactor deactivation caused by high syngas conversion rates or a low reactivity resulting in large unit sizes to achieve desired product quantities should be avoided. The design of the main operation point thus should be based on a complex techno-economical optimization to achieve the best trade-off between the relevant operation parameters.

A similar influence as with the temperature dependence can also be observed with the dependence on the H_2/CO ratio of the syngas feed shown in Figure 7. With increasing proportion of hydrogen, the CGP decreases and thus the share of light hydrocarbons increases, but in contrast to the reactor temperature, the setting of the H_2/CO ratio is subject to certain requirements in order to ensure uniform process operation, which result from the reactor operation itself. One common aim in the operation of FT reactors is to meet the reactors H_2/CO usage ratio with the H_2/CO syngas feed ratio [30] in order to maintain a constant proportion between the reactants throughout the entire reaction. Accordingly, even though the H_2/CO feed ratio has a relevant impact on the syncrude distribution and the reactor activity, its use as a controlling parameter is strongly limited in favor of a homogeneous synthesis process.

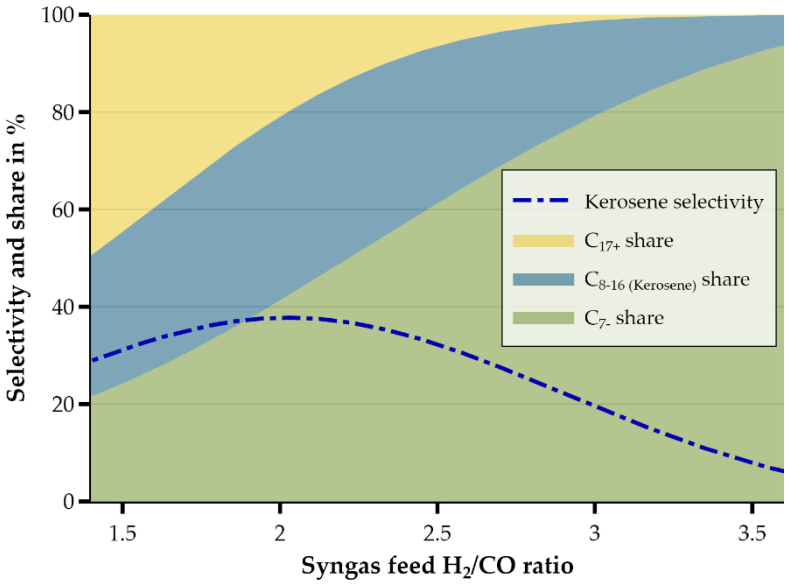

Figure 7. Syngas reactants ratio dependency on selectivity shares and kerosene range selectivity for a fixed bed reactor with T = 220 °C, p = 2.5 MPa and GHSV = 5 NL/h/g_{cat}.

Although mainly the reactor temperature has emerged as an authoritative control parameter which comes along with a high degree of freedom, the previous evaluations show the decisive possibilities to influence the syncrude composition and general reactor behavior by means of the key operation parameters. The impact on the upstream processes of the syngas generation results primarily from the feed gas composition which is required for a stable reactor operation at the desired operating point. The downstream processes, which include in particular the product separation and refining, are mainly affected by the reactor selectivity as their specific design should be based on the composition of the supplied syncrude.

4. Conclusion

 doi:10.20944/preprints202101.0564.v1

The presented work describes the process chain of a sustainable decentralized production of kerosene based on renewable energy and current technologies. According to general criteria that have to be met for decentralized fuel supply, the Power-to-Liquid process is selected as preferred option due to its flexible energy supply possibilities and minor impacts on land and water use in comparison to Biomass-to-Liquid processes.

As one of two possible process routes for a kerosene production based solely on electrical energy, synthesis via Fischer-Tropsch reaction is preferred to the other variant on account of its simple process structure and low refining effort. Relevant options for syngas generation are sketched and hydrocracking is selected as only refining step for the upgrading to an on-specification product. Based on a developed Python model for the simulation of a FT reactor, effects of the main operation parameters on product selectivity and reactor activity are provided to show the key position of the FT reactor as governing process in the production chain on the one hand, and its flexibility towards a targeted syncrude production on the other. The dependencies of the operation parameters and product composition on the reactor behavior represent the complex interrelationships in a FT. The product selectivity which is highly determined by the reactor temperature is decisive for the downstream processes of product separation and hydrocracking and the upstream processes due to its influence on the H_2/CO usage ratio which should be met by the H_2/CO syngas feed ratio. The influence of the reactor pressure and the GHSV on product selectivity and reaction activity is negligible. Those parameters can therefore be influenced by the overarching plant concept and are not solely governed by the FT process. However, as they both have a relevant impact on the syngas conversion whose range is crucial to meet a compromise between catalyst deactivation caused by increased water shares and process efficiency which is negatively affected by increasing amounts of unconverted syngas, a favorable reactor operation should be aimed at.

As a summary it might be stated that the presented reactor parameters offer high potential for a targeted process operation and the dependencies show the decisive role of the Fischer-Tropsch reactor for the PtL process. But since the FT reactor is also part of an overall system in the PtL process, a technical and/or economical process optimization towards a maximal process efficiency only can be performed under consideration of all relevant process steps.

5. Outlook

Future work will extend the Python model with additional process steps as well as internal and external gas recycles and relevant economic and operational parameters to depict the entire PtL production path from energy supply to the final product. On this basis both a process optimization for a decentralized production of kerosene and a system-analytical assessment of the future role of a sustainable kerosene production can be performed.

Author Contributions: Conceptualization, J.K. and A.M.; methodology, A.M.; software, A.M.; validation, A.M.; investigation, A.M.; writing—original draft preparation, A.M.; writing—review and editing, A.M, J.K.; visualization, A.M.; supervision, J.K.; project administration, J.K.; funding acquisition, J.K. All authors have read and agreed to the published version of the manuscript.

Funding: This research was funded by the German Federal Ministry for the Environment, Nature Conservation and Nuclear Safety via the project Klimaneutrale Alternative Kraftstoffe (ProQR) together with the Deutsche Gesellschaft für Internationale Zusammenarbeit (GIZ).

Conflicts of Interest: The authors declare no conflict of interest.

Appendix A. Table of notation

Preprints (www.preprints.org) | NOT PEER-REVIEWED | Posted: 27 January 2021 doi:10.20944/preprints202101.0564.v1

Table A1. Table of notation

Parameter	Description
AEL	Alkaline Electrolysis
ASF	Anderson-Schulz-Flory
AtJ	Alcohol-to-jet
BtL	Biomass-to-Liquid
CCU	Carbon Capture Usage
CGP	Chain growth probability [-]
Co-LTFT	Cobalt based low temperature Fischer-Tropsch
CSTR	Continuous stirred-tank reactor
DAC	Direct Air Capture
exp	Experimental
Fe-HTFT	Iron based high temperature Fischer-Tropsch
Fe-LTFT	Iron based low temperature Fischer-Tropsch
FT	Fischer-Tropsch
FT-SPK	Fischer-Tropsch Synthetic Paraffinic Kerosene
HTE	High temperature Electrolysis
PEM	Proton exchange membrane
PBtL	Power-Biomass-to-Liquid
PFR	Plug flow reactor
PREOS	Peng-Robinson equation of state
PtL	Power-to-Liquid
rWGS	Reverse Water-Gas Shift
SAF	Sustainable aviation fuel
SOEC	Solid oxide electrolysis cell
SPK	Synthetic Paraffinic Kerosene
StL	Sun-to-Liquid
TVS	Temperature-vacuum swing adsorption
a	Reaction order of partial pressure CO [-]
a_0	Adsorption coefficient at 493.15 K [-]
b	Reaction order of partial pressure H_2 [-]
c	Concentration [%]
d	Paraffin to olefin ratio constant [-]
E_a	Activation energy [J/mol]
err	Error [%]
GHSV	Gas hourly space velocity [NL/(s $g_{catalyst}$)]
k_0	Reaction rate constant at 493.15 K [-]
k_a	Rate constant of ratio of termination and propagation [-]
k_{CH4}	Temperature dependent reaction rate constant of methane [-]
k_{FT}	Temperature dependent reaction rate constant of FT products [-]
M	Molar fraction [-]
m_{cat}	Catalyst mass [g]
m_{mol}	Molar mass [g/mol]
$\dot{N}$	Particle flow [mol/s]
n	Carbon number [-]
p	Pressure [MPa]
q	Water effect constant [-]

Preprints (www.preprints.org) | NOT PEER-REVIEWED | Posted: 27 January 2021 doi:10.20944/preprints202101.0564.v1

R	Universal gas constant [(kg m²)/(s² mol K)]
R^2	Coefficient of determination [-]
r	Reaction rate [mol/(s $g_{catalyst}$)]
S	Selectivity [-]
T	Temperature [K]
t	Temperature [°C]
u	Conversion [-]
ur	Usage ratio [-]
$\dot{V}$	Volume flow [NL/h]
α	Chain growth probability [-]
β	Syngas ratio power constant [-]
Δ	Difference [-]

Appendix B. Reaction rate comparison

Table B1 shows the experimental derived reaction rates by [48, 49] for various reactor conditions with variations in syngas composition, system pressure and space velocity and the corresponding modeled reaction rates.

Table B1. Comparison of experimental [48, 49] and modeled reaction rates

Run	p_{CO} [MPa]	p_{H_2} [MPa]	GHSV [NL/g/h]	$r_{FT,exp}$ [mol/g/h]	$r_{CH_4,exp}$ [mol/g/h]	$r_{FT,model}$ [mol/g/h]	$r_{CH_4,model}$ [mol/g/h] [a]	err_{FT} [%] [b]	err_{CH_4} [%] [b]
2	0.710	1.420	16.0	0.0205	0.0022	0.0193	0.0020	5.85	8.02
3	0.710	1.420	10.0	0.0207	0.0021	0.0189	0.0019	8.70	12.63
4	0.710	1.420	6.0	0.0204	0.0019	0.0182	0.0017	10.93	14.86
5	0.710	1.420	3.0	0.0188	0.0016	0.0166	0.0012	11.49	30.09
7	0.710	1.065	16.0	0.0178	0.0015	0.0150	0.0014	15.51	6.82
8	0.710	1.065	10.0	0.0151	0.0014	0.0147	0.0013	2.72	7.14
9	0.710	1.065	3.0	0.0129	0.0011	0.0129	0.0008	-0.08	23.78
10	0.710	1.065	6.0	0.0145	0.0013	0.0141	0.0011	2.55	10.35
12	0.710	0.710	16.0	0.0100	0.0008	0.0105	0.0008	-5.50	3.23
13	0.710	0.710	10.0	0.0112	0.0008	0.0103	0.0008	7.77	2.50
14	0.710	0.710	3.0	0.0099	0.0006	0.0091	0.0005	7.78	12.39
15	0.710	0.710	6.0	0.0111	0.0007	0.0010	0.0007	10.36	5.46
17	0.487	1.217	16.0	0.0226	0.0025	0.0192	0.0023	15.31	7.40
18	0.487	1.217	10.0	0.0206	0.0025	0.0188	0.0022	8.79	11.23
19	0.487	1.217	3.0	0.0199	0.0022	0.0171	0.0015	14.23	31.99
20	0.487	1.217	6.0	0.0192	0.0023	0.0182	0.0020	5.10	14.69
22	0.608	1.217	16.0	0.0175	0.0021	0.0178	0.0019	-1.60	9.85
23	0.608	1.217	10.0	0.0172	0.0021	0.0174	0.0018	-1.10	14.46
24	0.608	1.217	6.0	0.0175	0.0019	0.0168	0.0016	4.17	16.56
25	0.608	1.217	3.0	0.0182	0.0016	0.0154	0.0011	15.16	27.75
27	0.811	1.217	16.0	0.0157	0.0015	0.0162	0.0015	-3.06	6.33
28	0.811	1.217	10.0	0.0184	0.0015	0.0158	0.0014	14.18	8.06
29	0.811	1.217	6.0	0.0148	0.0013	0.0151	0.0012	-2.30	11.31
30	0.811	1.217	3.0	0.0141	0.0010	0.0138	0.0008	2.48	20.13

[a] The methane reaction rate was calculated via the provided CH_4 selectivity [48].

[b] Error = $(r_{x,exp} - r_{x,model}) / r_{x,exp}$

The measurements were performed at a reactor temperature of 220 °C. As there is no continuous information regarding the total system pressure provided for each calculation run, the model reactor pressure was considered as the sum of the reported hydrogen and carbon monoxide partial pressures. The parity plots of both reaction rates are shown in Figure 8 for the modeled values and the rates calculated by Ma et al. [48, 49]. With coefficients of determination of $R^2 = 0.904$ for the FT reaction rate $r_{FT,model}$ and $R^2 = 0.930$ for

Preprints (www.preprints.org) | NOT PEER-REVIEWED | Posted: 27 January 2021 doi:10.20944/preprints202101.0564.v1

the methane reaction rate $r_{CH_4,model}$, the model still provides an adequate representation of the experimental results. The modeled results further show the expected behavior with changed process parameters. Deviations from the calculated values provided by [48, 49] mainly result from additionally modeled process-related influences on the chain growth probability, an additional consideration of olefins and the aforementioned uncertain deviation between the reactants partial pressures and the total reactor pressure.

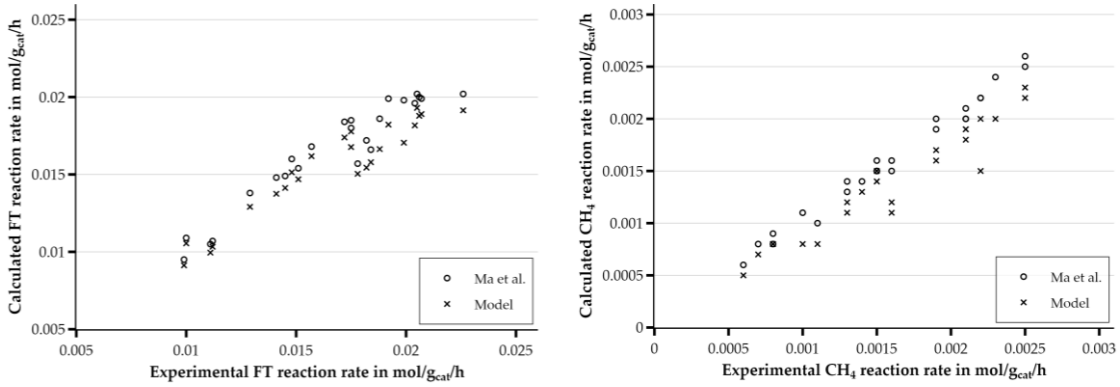

(**a**) (**b**)

Figure 8. Parity plots for the modeled and literature-based [48, 49] **(a)** FT reaction rates and **(b)** methane reaction rates.

References

1. Airbus; Global Market Forecast. **2019**.
2. REN21; Renewables Global Status Report. **2019**.
3. ICCT; Long-term aviation fuel decarbonization: Progress, roadblocks, and policy opportunities. **2019**, International Council on Clean Transportation.
4. IRENA; Biofuels for aviation: Technology brief. **2017**, International Renewable Energy Agency: Abu Dhabi.
5. Schmidt, P., et al.; Power-to-Liquids as Renewable Fuel Option for Aviation: A Review. *Chemie Ingenieur Technik* **2018**, *90(1-2)*: p. 127-140, DOI: 10.1002/cite.201700129.
6. Mawhood, R., et al.; Production pathways for renewable jet fuel: a review of commercialization status and future prospects. *Biofuels, Bioproducts and Biorefining* **2016**, *10(4)*: p. 462-484, DOI: 10.1002/bbb.1644.
7. Ail, S.S. and S. Dasappa; Biomass to liquid transportation fuel via Fischer Tropsch synthesis – Technology review and current scenario. *Renewable and Sustainable Energy Reviews* **2016**, *58*: p. 267-286, DOI: 10.1016/j.rser.2015.12.143.
8. Chiaramonti, D.; Sustainable Aviation Fuels: the challenge of decarbonization. in 10th International Conference on Applied Energy (ICAE2018). **2019**. Hong Kong, China.
9. Hileman, J.I. and R.W. Stratton; Alternative jet fuel feasibility. *Transport Policy* **2014**, *34*: p. 52-62, DOI: 10.1016/j.tranpol.2014.02.018.
10. Hamelinck, C., et al.; Production of FT transportation fuels from biomass; technical options, process analysis and optimisation, and development potential. *Energy* **2004**, *29(11)*: p. 1743-1771, DOI: 10.1016/j.energy.2004.01.002.
11. Sudiro, M. and A. Bertucco; Production of synthetic gasoline and diesel fuel by alternative processes using natural gas and coal: Process simulation and optimization. *Energy* **2009**, *34(12)*: p. 2206-2214, DOI: 10.1016/j.energy.2008.12.009.
12. Lee, H.-J., et al.; Conceptual Design of a Fischer–Tropsch Reactor in a Gas-to-Liquid Process. *Industrial & Engineering Chemistry Research* **2015**, *54(26)*: p. 6749-6760, DOI: 10.1021/acs.iecr.5b00556.
13. König, D.H., et al.; Simulation and evaluation of a process concept for the generation of synthetic fuel from CO_2 and H_2. *Energy* **2015**, *91*: p. 833-841, DOI: 10.1016/j.energy.2015.08.099.

14. Kirsch, H., et al.; CO_2-neutrale Fischer-Tropsch-Kraftstoffe aus dezentralen modularen Anlagen: Status und Perspektiven. *Chemie Ingenieur Technik* **2020**, *92(1-2)*: p. 91-99, DOI: 10.1002/cite.201900120.
15. Meurer, A., et al.; Fischer-Tropsch synthesis as key for decentralized sustainable kerosene production, in 15th Conference on Sustainable Development of Energy Water and Environment Systems - SDEWES. **2020**: Cologne, Germany.
16. ANP; Boletim de monitoramento da qualidade dos combustíveis. **2017**, Agência Nacional de Petróleo, Gás Natural e Biocombustíveis.
17. ASTM International; ASTM D1655-18, Standard Specification for Aviation Turbine Fuels. **2018**: West Conshohocken, DOI: 10.1520/d1655-18a.
18. Ministry of Defence; DEF STAN 91-091. **2011**, MODUK - British Defense Standards.
19. ASTM International; ASTM D7566-18, Standard Specification for Aviation Turbine Fuel Containing Synthesized Hydrocarbons. **2018**: West Conshohocken, DOI: 10.1520/d7566-18.
20. Holladay, J., Z. Abdullah, and J. Heyne; Sustainable Aviation Fuel. **2019**, Pacific Northwest National Laboratory.
21. Zschoke, A.; High Biofuel Blends in Aviation (HBBA). **2012**, Deutsche Lufthansa AG, Wehrwissenschaftliches Institut fur Werk- und Betriebsstoffe.
22. Gammon, J., ed.; Aviation Fuel Quality Control Procedures: 5th Edition. **2017**, ASTM International: West Conshohocken, PA, DOI: 10.1520/mnl5-5th-eb.
23. Marxer, D., et al.; Demonstration of the Entire Production Chain to Renewable Kerosene via Solar Thermochemical Splitting of H_2O and CO_2. *Energy & Fuels* **2015**, *29(5)*: p. 3241-3250, DOI: 10.1021/acs.energyfuels.5b00351.
24. Koepf, E., et al.; Liquid fuels from concentrated sunlight: An overview on development and integration of a 50 kW solar thermochemical reactor and high concentration solar field for the SUN-to-LIQUID project. *AIP Conference Proceedings* **2019**, *2126(1)*, DOI: 10.1063/1.5117692.
25. Umweltbundesamt; Power-to-Liquids - Potentials and Perspectives for the Future Supply of Renewable Aviation Fuel. **2016**.
26. Bundesamt für Justiz; Verordnung über Anforderungen an eine nachhaltige Herstellung von Biokraftstoffen (Biokraftstoff-Nachhaltigkeitsverordnung -Biokraft-NachV). **2018**.
27. European Union; Directive (EU) 2018/2001 of the European Parliament and of the Council of 11 December 2018 on the promotion of the use of energy from renewable sources (Text with EEA relevance.), in PE/48/2018/REV/1. **2018**: Official Journal of the European Union.
28. Government of Brazil; Presidential declaration No. 6961. **2009**.
29. Government of Brazil; Presidential declaration No. 7172. **2010**.
30. de Klerk, A.; Fischer-Tropsch Refining. **2011**: Wiley-VCH Verlag GmbH & Co. KGaA.
31. International Energy Agency; The Future of Hydrogen - Seizing today's opportunities. **2019**, International Energy Agency.
32. Sunfire GmbH; Durchbruch für Power-to-X. **2019**. Available online: https://www.sunfire.de/de/unternehmen/news/detail/durchbruch-fuer-power-to-x-sunfire-nimmt-erste-co-elektrolyse-in-betrieb-und-startet-die-skalierung (accessed on 09.04.2020).
33. Koytsoumpa, E.I., C. Bergins, and E. Kakaras; The CO_2 economy: Review of CO_2 capture and reuse technologies. *The Journal of Supercritical Fluids* **2018**, *132*: p. 3-16, DOI: 10.1016/j.supflu.2017.07.029.
34. Climeworks; Climeworks launches world's first commercial plant to capture CO_2 from air. **2017**. Available online: http://www.climeworks.com/wp-content/uploads/2017/05/01_PR-Climeworks-DAC-Plant-Opening.pdf (accessed on 14.04.2020).
35. Wurzbacher, J.A., et al.; Heat and mass transfer of temperature–vacuum swing desorption for CO_2 capture from air. *Chemical Engineering Journal* **2016**, *283*: p. 1329-1338, DOI: 10.1016/j.cej.2015.08.035.
36. Pastor-Pérez, L., et al.; CO_2 valorisation via Reverse Water-Gas Shift reaction using advanced Cs doped Fe-Cu/Al_2O_3 catalysts. *Journal of CO_2 Utilization* **2017**, *21*: p. 423-428, DOI: 10.1016/j.jcou.2017.08.009.

37. Stoots, C.M., et al.; Syngas Production via High-Temperature Coelectrolysis of Steam and Carbon Dioxide. *ASME. J. Fuel Cell Sci. Technol.* **2009**, *6(011014)*, DOI: 10.1115/1.2971061.
38. Daza, Y.A. and J.N. Kuhn; CO_2 conversion by reverse water gas shift catalysis: comparison of catalysts, mechanisms and their consequences for CO_2 conversion to liquid fuels. *RSC Advances* **2016**, *6(55)*: p. 49675-49691, DOI: 10.1039/c6ra05414e.
39. de Klerk, A.; Fischer–Tropsch fuels refinery design. *Energy & Environmental Science* **2011**, *4(4)*, DOI: 10.1039/c0ee00692k.
40. Chevron; Alternative Jet Fuels - A supplement to Chevron's Aviation Fuels Technical Review. **2006**, Chevron.
41. de Klerk, A.; Fischer–Tropsch refining: technology selection to match molecules. *Green Chemistry* **2008**, *10(12)*, DOI: 10.1039/b813233j.
42. Liu, Y., et al.; Selective Hydrocracking of Fischer–Tropsch Waxes to High-quality Diesel Fuel Over Pt-promoted Polyoxocation-pillared Montmorillonites. *Topics in Catalysis* **2009**, *52(6-7)*: p. 597-608, DOI: 10.1007/s11244-009-9239-8.
43. Yaws, C.L.; Critical Properties and Acentric Factor – Organic Compounds, in Thermophysical Properties of Chemicals and Hydrocarbons. **2014**. p. 1-124, DOI: 10.1016/b978-0-323-28659-6.00001-x.
44. Peng, D.-Y. and D.B. Robinson; A New Two-Constant Equation of State. *Ind. Eng. Chem. Fundamen.* **1976**, *15*: p. 59-64, DOI: 10.1021/i160057a011.
45. Anderson, R.B.; Catalysts for the Fischer-Tropsch Synthesis. *Catalysis* **1956**, *4*: p. 29-255.
46. Vervloet, D., et al.; Fischer–Tropsch reaction–diffusion in a cobalt catalyst particle: aspects of activity and selectivity for a variable chain growth probability. *Catalysis Science & Technology* **2012**, *2(6)*, DOI: 10.1039/c2cy20060k.
47. Iglesia, E., et al.; Selectivity Control and Catalyst Design in the Fischer-Tropsch Synthesis: Sites, Pellets, and Reactors. **1993**. p. 221-302, DOI: 10.1016/s0360-0564(08)60579-9.
48. Ma, W., et al.; Fischer–Tropsch Synthesis: Kinetics and Water Effect on Methane Formation over 25%Co/γ-Al_2O_3 Catalyst. *Industrial & Engineering Chemistry Research* **2014**, *53(6)*: p. 2157-2166, DOI: 10.1021/ie402094b.
49. Ma, W., et al.; Fischer–Tropsch synthesis: Kinetics and water effect study over 25%Co/Al2O3 catalysts. *Catalysis Today* **2014**, *228*: p. 158-166, DOI: 10.1016/j.cattod.2013.10.014.
50. Mahmoudi, H., et al.; A review of Fischer Tropsch synthesis process, mechanism, surface chemistry and catalyst formulation. *Biofuels Engineering* **2017**, *2(1)*: p. 11-31, DOI: 10.1515/bfuel-2017-0002.
51. Yang, J., et al.; Fischer–Tropsch synthesis: A review of the effect of CO conversion on methane selectivity. *Applied Catalysis A: General* **2014**, *470*: p. 250-260, DOI: 10.1016/j.apcata.2013.10.061.
52. Tucker, C.L., M. Claeys, and E. van Steen; Decoupling the deactivation mechanisms of a cobalt Fischer–Tropsch catalyst operated at high conversion and 'simulated' high conversion. *Catalysis Science & Technology* **2020**, *10(20)*: p. 7056-7066, DOI: 10.1039/d0cy00929f.